catalysts

MDPI

Article

Co-Production of Methanol and Methyl Formate via Catalytic Hydrogenation of CO_2 over Promoted Cu/ZnO Catalyst Supported on Al_2O_3 and SBA-15

Nor Hafizah Berahim, Noor Asmawati Mohd Zabidi * and Nur Amirah Suhaimi

Center of Contaminant Control and Utilization (CenCoU), Institute of Contaminant Management for Oil and Gas, Department of Fundamental and Applied Sciences, Universiti Teknologi PETRONAS, Seri Iskandar 32610, Malaysia

* Correspondence: noorasmawati_mzabidi@utp.edu.my; Tel.: +60-5-368-7675

Abstract: Cu/ZnO catalysts promoted with Mn, Nb and Zr, in a 1:1:1 ration, and supported on Al_2O_3 (CZMNZA) and SBA-15 (CZMNZS) were synthesized using an impregnation method. The catalytic performance of methanol synthesis from CO_2 hydrogenation was investigated in a fixed-bed reactor at 250 °C, 22.5 bar, GHSV 10,800 mL/g·h and H_2/CO_2 ratio of 3. The CZMNZA catalyst resulted in higher CO_2 conversion and MeOH selectivity of 7.22% and 32.10%, respectively, despite having a lower BET surface area and pore volume compared to CZMNZS. Methyl formate is the major product obtained over both types of catalysts. The CZMNZA is a promising catalyst for co-producing methanol and methyl formate via the CO_2 hydrogenation reaction.

Keywords: Al_2O_3; SBA-15; methanol; CO_2 hydrogenation; Cu/ZnO; methyl formate

check for updates

Citation: Berahim, N.H.; Mohd Zabidi, N.A.; Suhaimi, N.A. Co-Production of Methanol and Methyl Formate via Catalytic Hydrogenation of CO_2 over Promoted Cu/ZnO Catalyst Supported on Al_2O_3 and SBA-15. *Catalysts* **2022**, *12*, 1018. https://doi.org/10.3390/catal12091018

Academic Editor: Wanbing Gong

Received: 27 July 2022
Accepted: 1 September 2022
Published: 8 September 2022

Publisher's Note: MDPI stays neutral with regard to jurisdictional claims in published maps and institutional affiliations.

Copyright: © 2022 by the authors. Licensee MDPI, Basel, Switzerland. This article is an open access article distributed under the terms and conditions of the Creative Commons Attribution (CC BY) license (https://creativecommons.org/licenses/by/4.0/).

1. Introduction

As the world population increases and puts more pressure on limited fossil fuels, the solution to the imminent energy and environmental dilemmas becomes more crucial and the exploration of renewable energy receives more attention. The extensive use of renewable energy sources will eventually lead to a substantial reduction in the emissions of carbon dioxide, the primary cause of global warming and climate change [1,2]. Converting CO_2 into valuable and usable fuels and chemicals is one of the vital solutions in addressing and alleviating the major energy and environmental issues. Synthesis of methanol via catalytic CO_2 hydrogenation is receiving growing attention these days, not only because methanol is a key chemical platform, but also because of its use as a potential chemical storage carrier for excess H_2 produced from renewable energies and as a greenhouse gas recycling solution [3,4].

Methanol synthesis has been carried out industrially on Cu—ZnO/Al_2O_3 catalysts at 220–300 °C and 5–10 MPa for several decades, feeding 5–10% CO_2 into syngas streams [5]. Nevertheless, methanol can be obtained by the hydrogenation of CO_2 with speeds and carbon consumption factors equivalent to those of the conventional route [6]. The activation of CO_2 only occurs at a temperature higher than 200 °C at a sufficient rate. Under these conditions, the selectivity and yield of methanol decreases due to the formation of by products, such as CO, hydrocarbons, and alcohols. Therefore, it is crucial to develop catalysts with high methanol selectivity [7,8]. A copper catalyst is primarily used for CO_2 hydrogenation to methanol due to its excellent hydrogenation efficiency and low cost [9]. Furthermore, the research study shows that copper is the preferred metal and exhibits relevance for this reaction in the presence of ZnO due to synergic contact between Cu and ZnO [10]. The basic sites of ZnO in close contact with Cu sites will enhance the adsorption of CO_2 and ZnO also increases the Cu dispersion, which improved the catalytic activity. Apart from the metallic active sites, the support can also play a vital role in modulating and

enhancing the catalyst's efficiency. The most common supports used for methanol synthesis are metal oxides. Their properties greatly influence the performance of the catalyst [11]. In addition, since methanol synthesis on a Cu-based catalyst is a structurally sensitive reaction, it is beneficial to adjust its efficiency using different promoters that could boost the catalyst's performance, selectivity, or stability. Thus, many supports and promoters, such as CNTs [12], zeolite [13], mesoporous silica [14], Nb [15], Mn [16], Ce [17], Ag [18], Mg [19] etc., have been explored for methanol catalyst enhancement.

Li et al. [20] combined the high BET surface area and thermal stability of Al_2O_3 with the basicity of CeO_2 using a Cu/AlCeO catalyst to make a series of very efficient catalysts. The catalytic performances of Cu/Al_2O_3, Cu/CeO_2, and Cu/AlCeO were compared to assess the performance of the Cu/AlCeO catalyst at a pressure of 30 bar, temperature 200–280 °C and a GHSV of 14,400 mL/g.h. The CO_2 conversion rates for Cu/Al_2O_3, Cu/AlCeO, and Cu/CeO_2 were 1.5, 2.9, and 1.2% at 200 °C, and 19.9, 23.7, and 13.9% at 280 °C, respectively. Both CO_2 conversion and methanol selectivity were shown to be sensitive to reaction temperature. When using a Cu/AlCeO catalyst, selectivity was at its maximum (85%) at 200 °C and at its lowest (22%) at 280 °C. The results demonstrated the Cu/AlCeO catalyst exhibits a synergistic effect between Al_2O_3 and CeO_2, which was used as a support for the Cu-based catalyst. Huang et al. [21] developed a Cu/ZnO plate catalyst, utilizing a ZnO plate and tested its performance during CO_2 hydrogenation using different reducing gases (5 vol% CO-Ar, 2.5 vol% H_2/2.5 vol% CO-Ar, and 5 vol% H_2-Ar) at 300 °C for 6 h. The main objective of this research was to evaluate the synergistic effect between migrating Zn and Cu nanoparticles on the activity of methanol production. The reaction was carried out at 220–300 °C and 30 bar, and the catalytic performance was measured by the conversion and selectivity under circumstances with various reducing gas concentrations. At the same temperature, 5 vol% H_2 demonstrated the maximum performance, while 5 vol% CO showed the lowest performance. Likewise, with the same conversion, 5 vol% H_2 had the highest methanol selectivity, while 5 vol% CO had the lowest. Comparing 5 vol% H_2 to 5 vol% CO revealed a two-fold increase in CO_2 conversion and methanol yield. The smallest particle sizes were found in the catalyst with 5 vol% H_2. Nonetheless, CO_2 hydrogenation is not solely influenced by particle size. The shape of particles is also crucial. While poor performance catalysts have irregular shapes, high performance catalysts are spherical in shape.

The effect of ZnO and other metal oxide supports on the activity of methanol synthesis has been investigated by Fujitani [22]. Their investigations revealed that ZnO/SiO_2 has a synergistic effect with Cu/SiO_2 in the production of methanol. Without ZnO in the catalyst, the activity of the reaction did not vary as the reduction temperature increased, but the catalyst with ZnO exhibited a substantial increase. Increasing the amount of ZnO resulted in a larger synergistic effect in the reduction temperature range of 300 to 450 °C. However, the turnover frequency (TOF) for methanol synthesis reached its highest point at 0.19 of Zn and then began to decline above 0.20. There was no methanol synthesis activity found above 0.5. The synthesis of methanol required an activation energy of 83.7 kJ/mol when the zinc was at 0.19. On the other hand, it did not show any signs of a promoting effect for the RWGS reaction. The TOF for CO began to decline, particularly between 0.15 and 0.2 Zn, and reached zero at 0.5 Zn. Other metal oxides that display synergistic effects with the Cu-ZnO catalyst include Al_2O_3, Ga_2O_2, ZrO_2, and Cr_2O_3. Din et al. [23] investigated the effect of the ZrO_2 promoter employed in the Cu catalyst on the activity and physiochemical properties of carbon nanofibers (CNFs) in the synthesis of methanol. Five catalysts with varying concentrations of ZrO_2 (5, 10, 15, 20, and 25 wt.%) were synthesized. The performance of the catalyst was examined at 180 °C and 3 MPa with a H_2:CO_2 = 3:1. The degree of CuO crystallization was unaffected by the amount of ZrO_2; however, the amorphous form of Cu was affected. Maximum dispersion and lowest crystallization were observed when 15 wt.% ZrO_2 was added to the CuO catalyst. The 15 wt.% of ZrO_2 is optimal for the Cu/ZrO_2 catalyst because it has the highest surface area and the smallest particle size. In addition, the catalyst had the highest levels of methanol activity (25 g/kg_{cat}·h) and methanol selectivity

of 67%. Using 20 wt.% ZrO_2 resulted in slightly better CO_2 conversion, but the difference was less than 1%. In comparison to the previously reported Ag- and Pd-based catalysts, the current catalyst shows improved performance and reaction conditions.

Theoretically, the methanol synthesis reaction will produce an equal mole of methanol and water. Nevertheless, practically in most catalytic hydrogenation reactions, the formation of by-products cannot be avoided. The common by-products from methanol synthesis from CO_2 are, and not limited to, carbon monoxide, methyl formate, ethanol, and traces of methane. According to the findings of Chen et al. [24], the formation of CO is a significant by-product, and in the majority of instances, it is the only by-product that results from the parallel formate dissociation mechanism. Despite this, CO can be recycled back to the feed inlet. In addition, the formation of methyl formate (MF) can be considered a value-added by-product to the techno-economics of the process. MF is essential for defossilizing industries and transportation. This C1 building block permits the production of a vast array of daughter products, in addition to its use as a fuel or fuel additive. Using methanol as a fuel in internal combustion engines, for instance, necessitates the addition of methyl formate to ensure year-round use, even at low temperatures [25]. Hence, designing a catalyst for a specific targeted product (methanol), but at the same time producing a by-product (MF) that can add value to the economics of the process, is the purpose of this paper.

In this paper, Cu/ZnO catalysts supported on Al_2O_3 and SBA-15, with the addition of tri-promoters (Mn/Nb/Zr), were synthesized and characterized. The catalytic performance was evaluated for the hydrogenation of CO_2 to methanol.

2. Results and Discussion

Table 1 illustrates the textural properties of Al_2O_3 and SBA-15 bare supports and their respective promoted Cu/ZnO catalysts supported on Al_2O_3 (CZMNZA) and SBA-15 (CZMNZS). Surface areas (S_{BET}) and pore volumes (V_P) of Al_2O_3 and SBA-15 bare supports are reduced after metal oxide loading, indicating that the active phase was dispersed onto the support and filled the pores [26]. In contrast, the pore diameter increased after the metal oxide loading. It is possible that the particles closed the smaller pores preferentially during loading. In this manner, the average pore diameter increased while the pore volume decreased, because the only pore remaining for physisorption was the larger one.

Table 1. Textural properties of Al_2O_3 and SBA-15 bare supports and their impregnated catalysts.

Sample	S_{BET} (m^2/g)	V_P (cm^3/g)	D_{BJH} (nm)
Al_2O_3	134.51	0.26	5.29
CZMNZA	99.95	0.20	5.70
SBA-15	695.48	1.01	5.71
CZMNZS	319.79	0.73	7.86

Figures 1 and 2 show the nitrogen adsorption-desorption isotherms and pore size distributions for Al_2O_3 and SBA-15, respectively. The Al_2O_3 support and its impregnated sample exhibited type V isotherms with type H4 hysteresis loop isotherms. The type V isotherm is associated with mesoporous adsorbents, while the type H4 hysteresis is associated with slit-shaped pores [27]. The isotherms for the SBA-15 support and impregnated sample showed a classic type IV with an H2 type hysteresis loop. The sample has a slope adsorption branch and a steep desorption branch at high relative pressure ($P/Po \geq 0.6$). This is due to cavitation-induced evaporation or pore obstruction or percolation within a limited range of pore necks. The pore size distributions for all samples reveal that the diameter of all catalyst pores lies between 3 and 12 nm, indicating the existence of mesoporous structures.

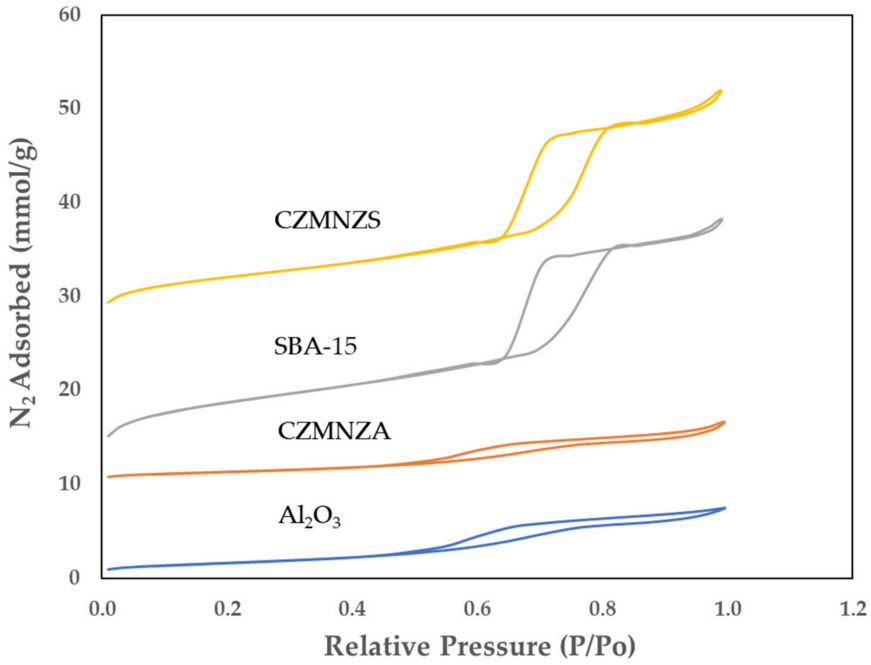

Figure 1. Nitrogen adsorption–desorption isotherms of the supports and catalysts.

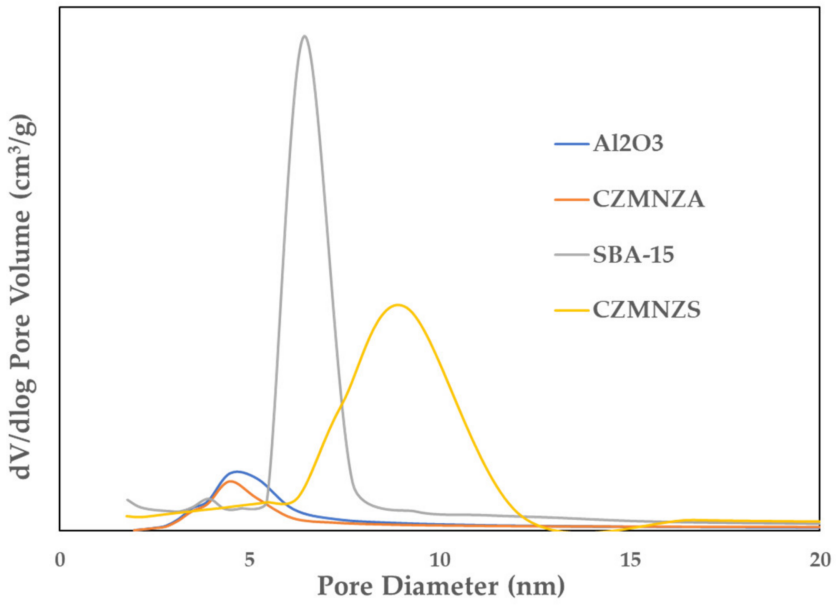

Figure 2. Pore size distributions of the supports and catalysts.

The morphologies of the Al_2O_3 and SBA-15 supports and their promoted Cu/ZnO catalysts were analyzed by FESEM, and the images are shown in Figure 3. The commercial Al_2O_3 support and its promoted Cu/ZnO catalyst exhibited irregular morphologies. The synthesized SBA-15 support showed a tubular shape. Adjusting the synthesis parameters of SBA-15, which include pH, synthesis duration, aging time, and washing solvent, enables the formation of the compound with a wide variety of geometries and morphologies. These include spherical and tubular forms, among others [28]. Both impregnated catalysts were unevenly dispersed onto the supports. Due to low levels of promoters used in the formulation, some promoters were not detectable in the samples, as revealed by the EDX mapping in Figure 4.

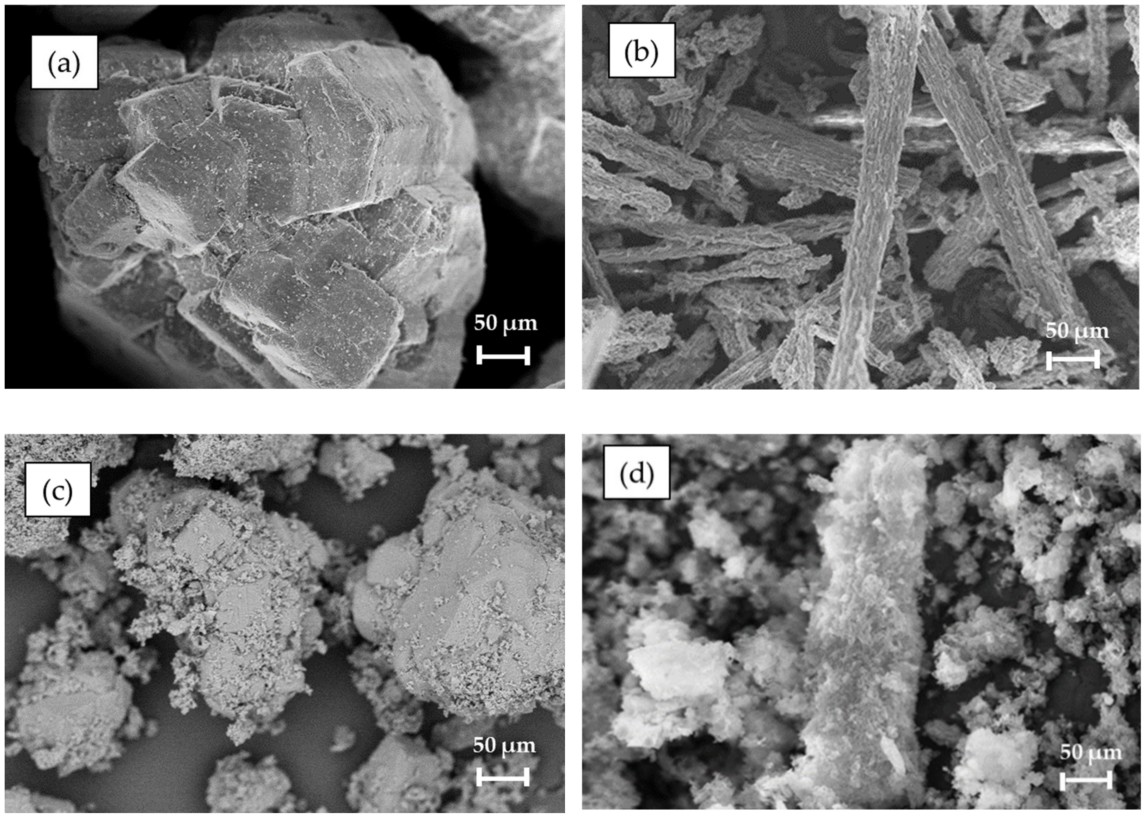

Figure 3. FESEM images of (**a**) Al_2O_3 (**b**) SBA-15 (**c**) CZMNZA (**d**) CZMNZS.

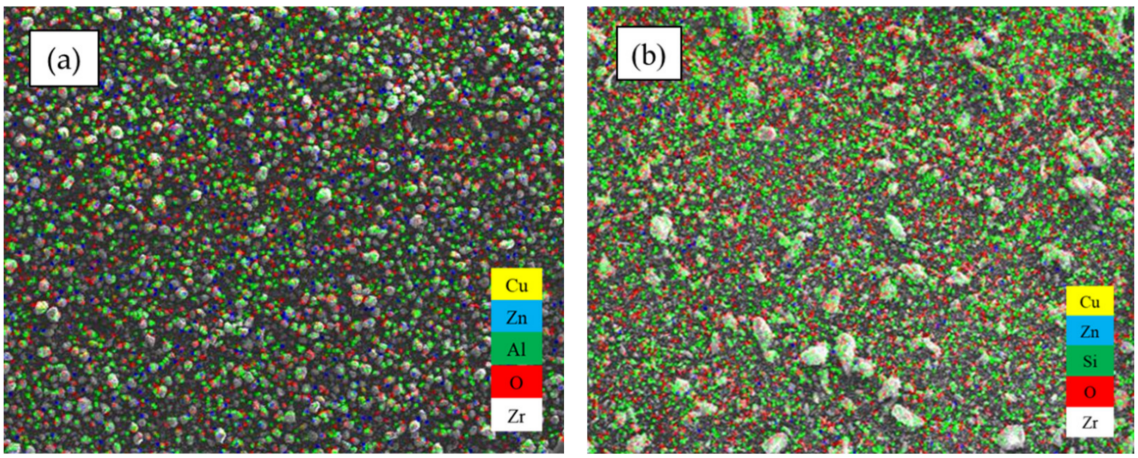

Figure 4. EDX mapping of (**a**) CZMNZA (**b**) CZMNZS.

TEM analysis was also performed for both loaded Cu/ZnO catalysts and the images are depicted in Figure 5, while the average particle size is shown in Table 2. The metal oxide nanoparticles appear to have irregular spherical and hexagonal shapes. The average metal particle size of CZMNZA is larger, 16.00 nm than that of CZMNZS, and was 6.09 nm. The size distribution curve (Figure 6) of the CZMNZA particles shift to the right, which corresponds to the direction of larger catalyst size, and becomes wider, while CZMNZS shows an opposite trend. Despite having the smallest particle size, the nanoparticles of CZMNZS were discovered to be deposited on the outer surface of SBA-15 rather than the inner channel of SBA-15 and some are severely agglomerated. The atomic composition of both catalysts is depicted in Table 3. The Cu/Zn ratio for both CZMNZA and CZMNZS

differ from the theoretical value (2.3), which suggest the inhomogeneity of the Cu and Zn species on the top surface of the catalysts.

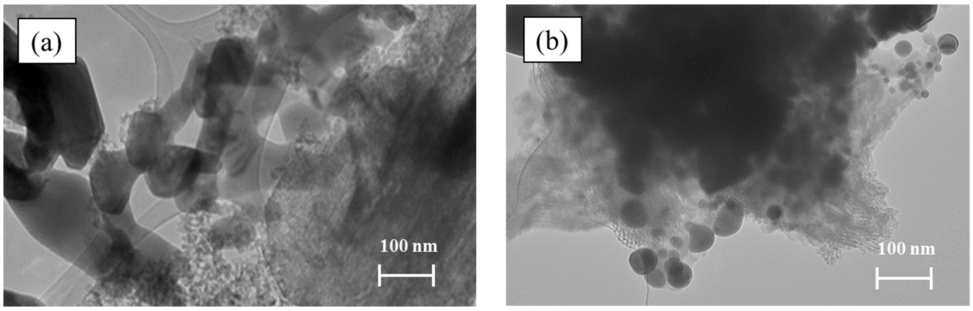

Figure 5. TEM images of (**a**) CZMNZA (**b**) CZMNZS.

Table 2. Average particle size of catalysts.

Sample	Average Particle Size (nm)
CZMNZA	16.00 ± 8.00
CZMNZS	6.09 ± 2.37

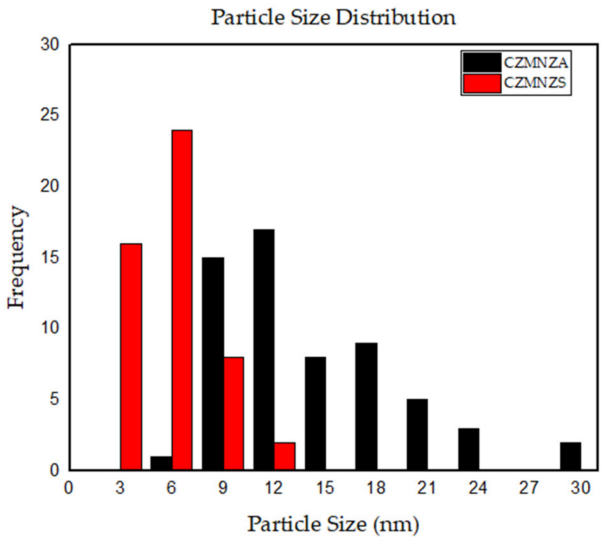

Figure 6. Particle size distribution of CZMNZA and CZMNZS.

Table 3. Atomic compositions of catalysts.

Catalyst	Atomic Composition (%)					Ratio
	Cu	Zn	Mn	Nb	Zr	Cu/Zn
CZMNZA	5.24	7.36	0.42	0.06	0.16	0.71
CZMNZS	8.07	5.95	1.93	0.09	0.17	1.36

XRD analysis was used to determine the phase composition and crystallographic structure of the catalyst. The XRD patterns of the Al_2O_3 bare support and CZMNZA are shown in Figure 7. Two major peaks can be observed at 2θ of 45.90° and 67.18°, which suggests the presence of gamma alumina (γ-Al_2O_3) [29], and the peaks are present in the diffraction peaks of the CZMNZA, which indicates the existence of alumina as a catalyst support. The CZMNZA sample had tenorite CuO peaks at 32.5°, 35.5°, 38.8°, 48.8°, 58.3°, 61.5°, 72.5°, and 75.2° [29]. Zincite, ZnO diffraction peaks, on the other hand, were found at 32.5° and 48.8° [29], albeit the peak may overlap with the CuO peaks [30,31].

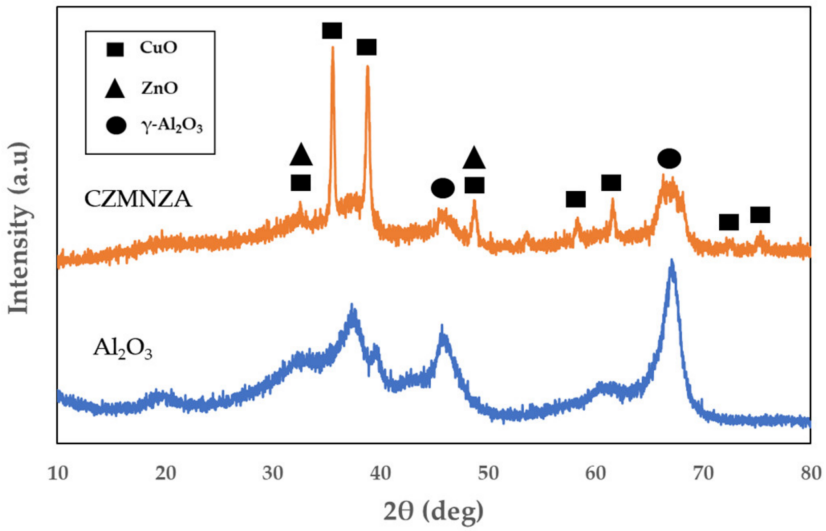

Figure 7. XRD patterns of Al_2O_3 and CZMNZA.

Figure 8 shows the low-angle XRD pattern of the SBA-15 bare support and CZMNZS. There are three well-resolved diffraction peaks associated with highly ordered mesoporous silica SBA-15, with two-dimensional hexagonal symmetry at 2θ = 0.89°, 1.6°, and 1.83° [32,33], which can be indexed as the (100), (110) and (200) diffractions, respectively, associated with highly ordered mesoporous silica SBA-15 with two-dimensional hexagonal symmetry (space group p6mm) [34]. The CZMNZS still displayed three indexed peaks, showing that adding metal precursors to SBA-15 did not cause the mesoscopic order of the two-dimensional hexagonal structure to collapse [35]. Despite this, due to the presence of metal precursor species in the SBA-15 channels, the intensity of the (100) diffraction peak was reduced. Figure 9 shows the XRD patterns of CZMNZA and CZMNZS. The wide-angle measurement of CZMNZS shows that the Cu-species were broadly distributed on the support. This finding was consistent with those of a prior work on CuO/SBA-15 [36]. Meanwhile, ZnO does not show a diffraction peak, most likely because it is amorphous or widely distributed in the sample [37].

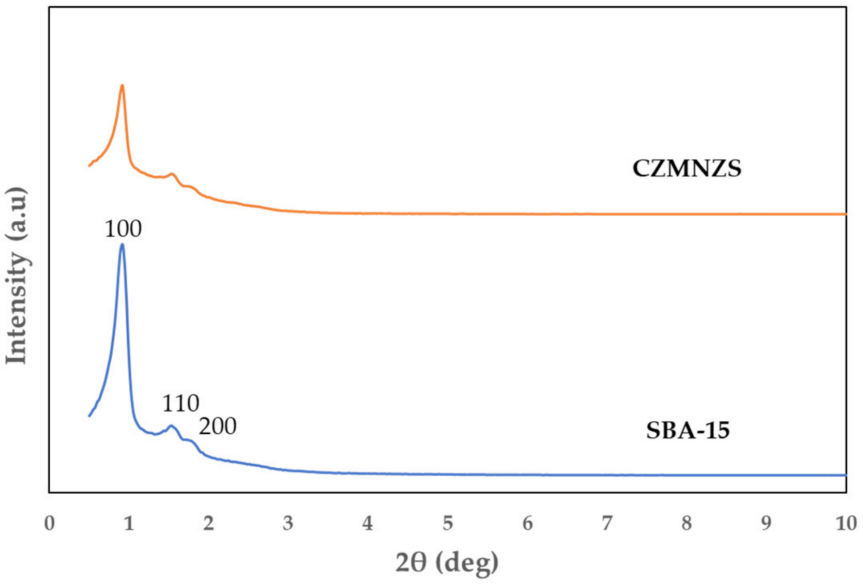

Figure 8. Low-angle XRD patterns of SBA-15 and CZMNZS.

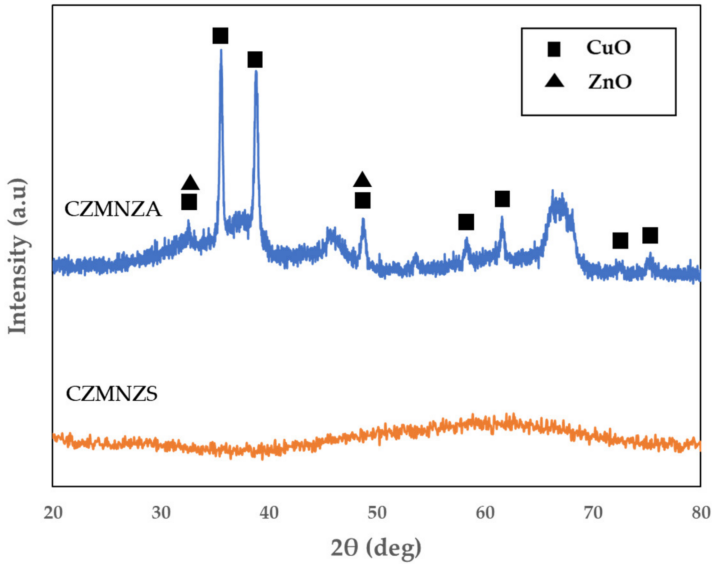

Figure 9. XRD patterns of CZMNZA and CZMNZS.

The ability of a catalyst to absorb hydrogen linearly with temperature will indicate its reducibility. The H_2-TPR profiles of CZMNZA and CZMNZS are depicted in Figure 10. The TPR profile of the CZMNZA catalyst exhibits only a single peak, indicating the presence of highly dispersed Cu species on the Al_2O_3 support, while the CZMNZS catalyst exhibits two peaks (α and β), which suggest that the catalysts contain both highly dispersed Cu species (α) and bulk-like Cu species (β) [38,39]. From the TPR profile, it can also be deduced that CZMNZA shifts to the left, exhibiting a lower reduction temperature, and indicating the higher reducibility of the catalyst active metals due to fewer metal oxides bound to the support. This is in accordance with the intrinsic reducibility theory that was mentioned by Jones et al. [40]. On the other hand, CZMNZS exhibits lower reducibility, which is shown by a higher reduction temperature, due to the formation of copper silicate from the amorphous Cu-containing particles, which can be observed in XRD [41]. Nevertheless, the reduction temperatures for both CZMNZA and CZMNZS stayed within the range of 200–400 °C. Table 4 shows the reduction temperature and total H_2 consumption for the CZMNZA and CZMNZS samples. Higher H_2 consumption for the CZMNZS, compared with that of CZMNZA, might be due to the enhanced H_2 spillover effect of the SBA-15 support.

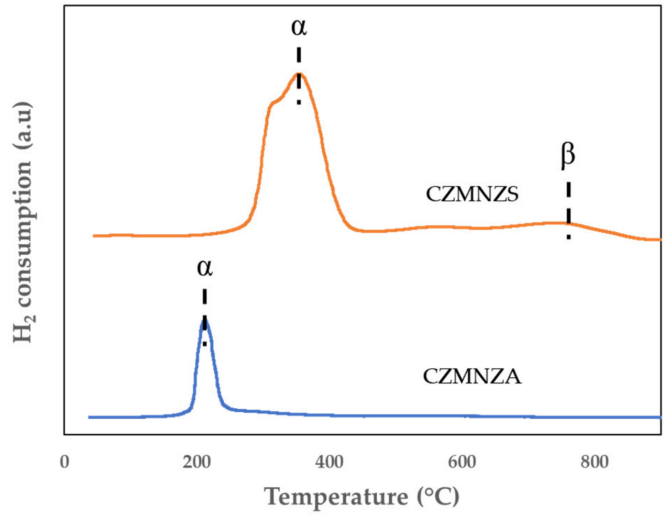

Figure 10. H_2-TPR profiles of CZMNZA and CZMNZS.

Table 4. H_2-TPR data of CZMNZA and CZMNZS.

Catalyst	Reduction Temperature (°C)		Total H_2 Consumption (μmol/g)
CZMNZA	213		717
	α	β	
CZMNZS	355	743	2329

Surface acidity has a significant impact on catalytic behavior and performance. NH_3-TPD analysis was used to determine the types of acid sites and surface acidity for the catalysts on different types of supports. NH_3-TPD profiles of the synthesized catalysts are shown in Figure 11. Typically, the desorption temperature of NH_3 can be used to classify the strength of solid acid sites within the TPD profiles as weak (120–300 °C), moderate (300–500 °C) and strong (>500 °C) [42]. Both catalysts display two temperatures of NH_3 desorption zones (350–450 °C) and (>500 °C), which represent moderate and strong acidic sites, respectively. The type of catalyst support influences the amount and the type of the acid sites. The CZMNZA shows higher amount of weak to moderate acidic sites than that of CZMNZS. Nevertheless, the CZMNZS exhibited a higher number of acidic sites, as compared to the CZMNZA sample.

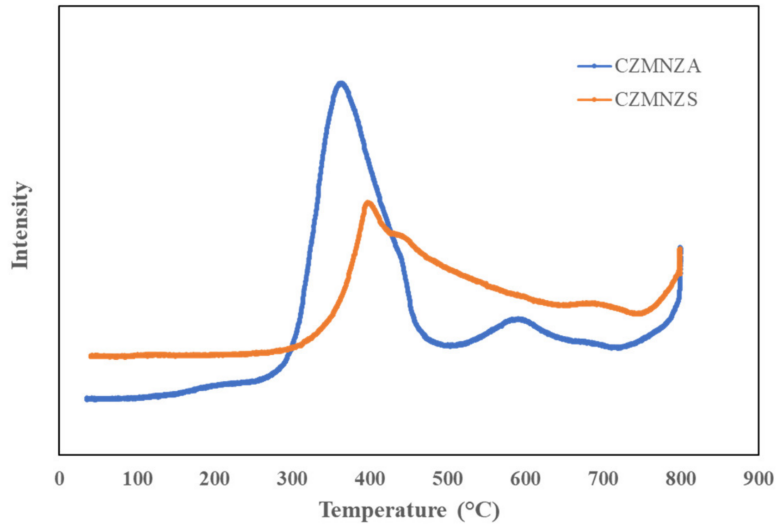

Figure 11. NH_3-TPD profiles of CZMNZA and CZMNZS.

The density and strength of the catalyst basic sites were measured using a CO_2-TPD technique. CO_2 gas was used in the experiment, which has sufficient acidity to probe all the basic sites in the samples. Figure 12 shows the CO_2-TPD profiles of CZMNZA and CZMNZS. The strength of basic sites is classified as weak basic sites, α (<200 °C), medium basic sites (200–550 °C), and strong basic sites (>500 °C) [43,44]. Given that the temperature of the reaction is maintained at less than 400 °C, it is anticipated that the basic sites will be associated with the active sites for the CO_2 hydrogenation reaction. The low temperature desorption peaks (<200 °C) are associated to the CO_2 species that have been absorbed onto the surface by weakly held hydroxyl groups and/or metal-oxygen pairs, such as Al–O, Zn–O, Mn–O, Nb–O and Zr–O [45]. Meanwhile, the high temperature desorption peak (>500 °C) is due to the coordinatively unsaturated O^{2-} ions that form because of the partial breakage of the metal-oxygen pair [45,46]. The CZMNZA catalyst showed all three desorption peaks, while the CZMNZS catalyst exhibited a single desorption peak with moderate basicity. The stronger basic sites for the CZMNZA catalyst at the temperature >500 °C may be attributable to its larger net electronic charge, which led to a lower degree of oxygen atom coordination [47]. Meanwhile, the low-temperature desorption peak at 134 °C was ascribed to the interaction of CO_2 with weak basic sites, which correspond to the OH^- groups on the catalyst surface [48].

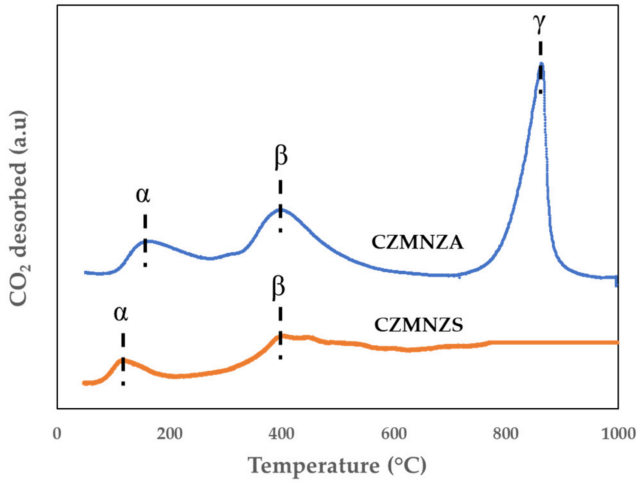

Figure 12. CO_2-TPD profiles for CZMNZA and CZMNZS.

The catalytic performance of Cu/ZnO supported on Al_2O_3 and SBA-15, loaded with tri-promoters (Mn/Nb/Zr) at an equal ratio, was evaluated at H_2:CO_2 = 3:1, 250 °C, 22.5 bar and GHSV 10,800 mL/g·h. The carbon-containing compounds obtained under these reaction conditions were methanol, methane, methyl formate and ethanol. The CZMNZA catalyst resulted in a higher CO_2 conversion from the hydrogenation reaction at 2.61% as compared to CZMNZS at 0.48%, as shown in Figure 13. For MeOH selectivity (Figure 14), CZMNZA also resulted in a higher value of 16.09%, compared to only 3.16% from that of the CZMNZS catalyst. Looking at the catalytic activity and selectivity over both catalysts, although the SBA-15-supported catalyst had higher BET surface area and pore volume compared to the Al_2O_3-supported catalyst, there is no direct relation between those properties and catalytic performance. This could be due to the active metals adhering to the outer surface of the SBA-15, rather than the inside of the mesoporous channels. Even though SBA-15 has a larger surface area than Al_2O_3, a significant loss of active sites may result in a drop in catalyst performance. Furthermore, with the damage of the pore system as a result of excessive silicate formation, particularly zinc silicate, and despite the small particle size and high Cu/Zn ratio compared to CZMNZA, CZMNZS possessed inaccessible Cu surface areas, which resulted in poor methanol synthesis activity [49]. Despite having a lower BET surface area and pore volume, Cu/ZnO supported on Al_2O_3 exhibits higher CO_2 conversion and MeOH selectivity compared to those of Cu/ZnO supported on SBA-15. Cu and ZnO agglomerates on the Al_2O_3 surface exposed more active sites to interact with the feed gases CO_2 and H_2, leading to increased methanol production [50]. In addition to that, the CZMNZA contains very strong basic sites, resulting in enhanced CO_2 conversion and methanol selectivity, since an increase in basicity has been shown to favor the synthesis of methanol [45,51]. The outstanding catalytic activity of CZMNZA, as compared to CZMNZS, can also be related to the reducibility of the catalyst. Prior to the experiment, the catalyst needs to be reduced to minimize surface active site aggregation. The CZMNZA demonstrated a lower reduction temperature than CZMNZS, thus is advantageous for enhancing copper dispersion and activity in methanol synthesis, as reported by Fujita et al. [52].

Apart from methanol, it can be observed from Figure 14 that the reaction favors the formation of methyl formate over both the supported catalysts. The following reaction could lead to the formation of methyl formate:

$$2CH_3OH \rightarrow C_2H_4O_2 + 2H_2 \quad (1)$$

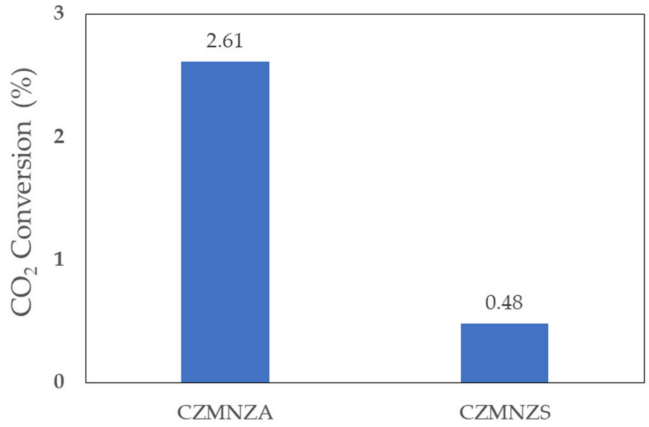

Figure 13. CO_2 conversion over Al_2O_3 and SBA-15-supported catalysts at reduction temperature 250 °C.

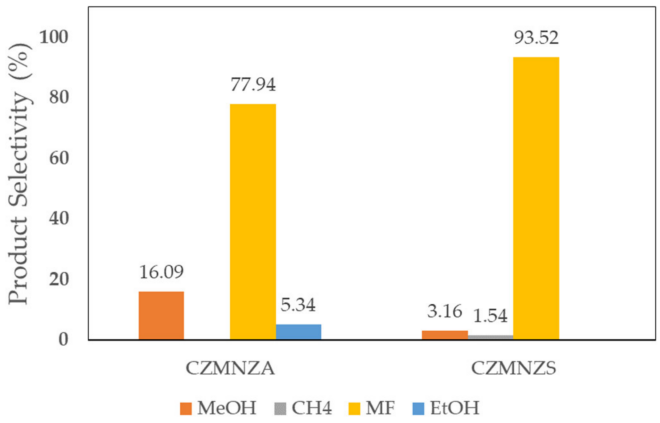

Figure 14. Product selectivity over Al_2O_3 and SBA-15-supported catalysts at reduction temperature 250 °C.

According to a previous work [52], the endothermic dehydrogenation of methanol to methyl formate occurs during methanol synthesis. It has also been reported that, depending on the composition of the catalyst, formates are converted to methoxy species at a different temperature and the latter is eventually hydrogenated into methanol. As the samples are heated, formic acid adsorption provides the hydrogen consumed for hydrogenation. Therefore, there is insufficient hydrogen for all formates to be converted into methoxy species. Since both formate and methoxy species were present at the same time on the surface of the catalyst, the mixed product methyl formate is obtained [53]. In addition to the dehydrogenation of methanol, other methods for MF formation include the base- or acid-catalyzed esterification of formic acid and methanol, as well as the reaction of methanol and carbon monoxide [54,55]. This statement supported the observed trend in which higher selectivity towards methyl formate was obtained compared to methanol over the CZMNZS and CZMNZA catalysts, which contained both acidic and basic sites, as shown by the NH_3-TPD and CO_2-TPD profiles. The CZMNZS catalyst also had a higher amount of acid sites compared to the CZMNZA catalyst, which led to higher selectivity towards methyl formate.

Figure 15 shows the time on stream (TOS) plot for CO_2 conversion, while Figure 16a,b show the time on stream plot (TOS) for product selectivity (MeOH and MF) to illustrate the pattern for CO_2 conversion as well as MeOH and MF formation during the 5 h reaction. It was noticed that CO_2 conversion for CZMNZA was high at the beginning of the reaction; however, after 50 min, it significantly dropped until the reaction was complete. For CZMNZS, the CO_2 conversion was stable throughout the 5 h reaction. A similar trend was observed for MeOH and MF formation for the CZMNZS. Nevertheless, CZMNZA shows

a different trend, where at the beginning of the reaction, the formation of MeOH and MF was almost similar, but after 50 min, the MeOH formation started to drop drastically, while MF formation slowly increased and stabilized over the 5 h of reaction duration.

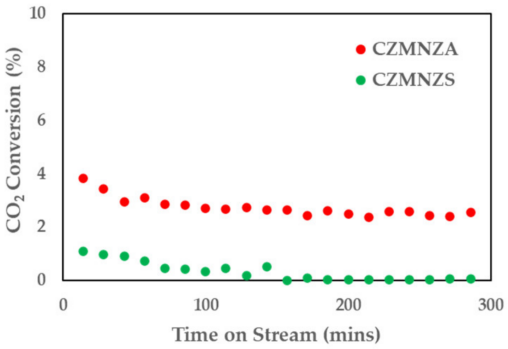

Figure 15. TOS of CO_2 conversion at reduction temperature 250 °C.

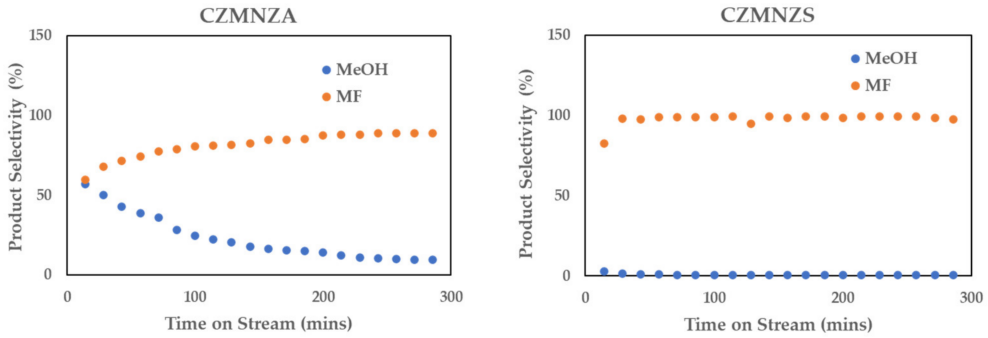

(**a**) (**b**)

Figure 16. TOS of methanol and methyl formate selectivity for (**a**) CZMNZA (**b**) CZMNZS at reduction temperature 250 °C.

The catalysts were also tested for their catalytic activity at the same reaction conditions as those mentioned but at a reduction temperature of 400 °C based on the TPR analysis of CZMNZS. The catalytic performance of CZMNZA and CZMNZS in terms of CO_2 conversion and products selectivity is shown in Table 5, while Figures 17 and 18 show the time on stream (TOS) plots for CO_2 conversion and product selectivity (MeOH and MF), respectively. The CZMNZA still shows the higher CO_2 conversion and MeOH selectivity of 7.22% and 32.10%, respectively. Among the products formed, MF resulted in the highest selectivity, regardless of the reduction temperature used; however, it decreased in value. The TOS for CO_2 conversion and product selectivity (MeOH and MF) of CZMNZA and CZMNZS at a higher reduction temperature (400 °C) shows the same trend as that of the lower reduction temperature (250 °C). The higher reduction temperature increased the CO_2 conversion for both catalysts and increased the MeOH selectivity of CZMNZA; however, it decreased the MeOH selectivity of CZMNZS.

Table 5. Catalytic activity of CZMNZA and CZMNZS at reduction temperature 400 °C.

Catalyst	CO_2 Conversion * (%)	Product Selectivity * (%)			
		MeOH	CH_4	MF	EtOH
CZMNZA	7.22	32.10	-	64.57	1.99
CZMNZS	4.39	2.60	-	91.65	5.74

* Reaction conditions: 250 °C, 22.5 bar, H_2:CO_2 = 3:1, GHSV 10,800 mL/g·h.

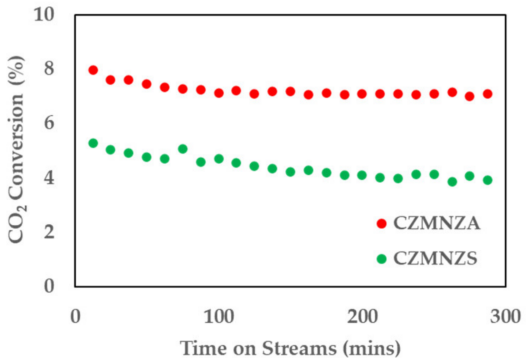

Figure 17. TOS of CO_2 conversion at reduction temperature 400 °C.

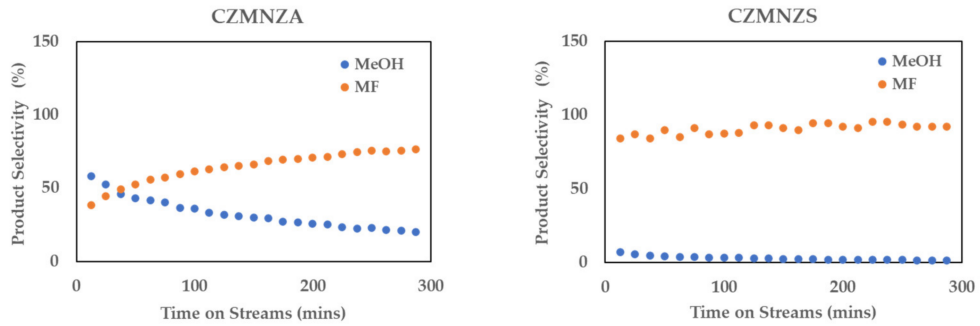

(**a**) (**b**)

Figure 18. TOS of methanol and methyl formate selectivity for (**a**) CZMNZA (**b**) CZMNZS at reduction temperature 400 °C.

3. Materials and Methods

3.1. Catalyst Preparation

3.1.1. Preparation of Catalyst Supports (Al_2O_3 and SBA-15)

Al_2O_3, which was commercially purchased from Merck, was treated under argon flow at 400 °C for 5 h to remove moisture and impurities.

The SBA-15 was synthesized using the nonionic triblock copolymer surfactant template. Then, 5 g of pluronic 123 (P123) (5800 g/mol) triblock copolymer was dissolved in 37.5 mL deionized water and placed in a 500 mL polypropylene (PP) bottle. A large stir bar was added to afford adequate stirring. The PP bottle was placed in a regulated oil bath at 40 °C on a hot plate stirrer. Next, 150 mL of 2M HCl solution was added to the P123 solution and stirred for 3 h at 40 °C and 10 g tetraethyl orthosilicate (TEOS, 208.33 g/mol) was added dropwise into the stirred P123 solution and the reaction proceeded for 24 h at 40 °C. Then, the bottle containing the mixture was placed in an oven at 95 °C for 48 h. Next, the precipitate was placed in the Buchner funnel and washed with 1125 mL deionized water, followed by 110 mL of ethanol. The precipitate was dried overnight in an oven at 90 °C, ground to fine powder and calcined at 600 °C for 6 h [28].

3.1.2. Preparation of Cu/ZnO-Based Catalyst with the Addition of Promoters

Cu/ZnO (70:30) with a fixed metal loading of 15 wt.% and promoters (Mn/Nb/Zr) with ratio of 1:1:1 and total loading of 0.09 wt.% was synthesized using the wetness impregnation method. The amounts of each precursor and promoter added were calculated based on the amount of total catalyst mass prepared.

Firstly, a specified amount of copper (II) nitrate trihydrate ($Cu(NO_3)_2{\cdot}3H_2O$), zinc nitrate hexahydrate ($Zn(NO_3)_2{\cdot}6H_2O$), manganese (II) nitrate tetrahydrate ($Mn(NO_3)_2{\cdot}4H_2O$), ammonium niobate (V) oxalate hydrate ($C_4H_4NNbO_9{\cdot}xH_2O$) and zirconium (IV) oxynitrate hydrate ($ZrO(NO_3)_2{\cdot}H_2O$) were dissolved in a desired amount of deionized water to form

0.5 M aqueous precursor solution. The solution was stirred for 1 h to ensure homogeneity. Then, the prepared aqueous precursor solution was added dropwise into a beaker containing the supports (Al_2O_3 and SBA-15). The pH of the solution was kept at 7 by adding 10% ammonia solution or 10% nitric acid solution. After 24 h of stirring, the solution was filtered and washed with deionized water. The produced paste was dried for 12 h at 120 °C and calcined for 4 h at 350 °C.

Cu/ZnO/Mn/Nb/Zr/Al_2O_3 and Cu/ZnO/Mn/Nb/Zr/SBA-15 catalyst samples were denoted as CZMNZA and CZMNZS, respectively.

3.2. Catalyst Characterization

The morphologies of the samples were examined using the Hitachi SU8020 field emission scanning electron microscope (FESEM). Textural analysis was carried out on a Micromeritics ASAP 2020 analyzer by determining the nitrogen adsorption/ desorption isotherms at −196 °C. The samples were degassed at 350 °C (heating rate 10 °C/min) prior to analysis. The adsorption data were used to calculate the Brunauer-Emmett-Teller (BET) specific surface area and pore volume. The Barrett-Joyner-Halenda (BJH) model was used to calculate the mean pore diameter of the isotherm desorption branch [24]. The catalyst component and phase study were determined using X-ray diffraction (XRD) from Shimadzu XRD-7000. The XRD measurements were performed at room temperature and ranged from 10° to 80° Bragg angle for the alumina samples, 0.5° to 10° for the SBA-15 bare support, and 0.5° to 80° for the impregnated SBA-15 sample. The reducibility of metal oxides was conducted using a Thermo Finnigan TPD/R/O 110 CE instrument, equipped with a thermal conductivity detector (TCD). Then, 40 mg of catalyst was pre-treated with N_2 at 250 °C for 1 h to eliminate moisture and impurities. The analysis continued with 5% H_2/Ar (20 mL/min) gas flow to 950 °C, with a 10 °C/min ramping rate and holding for an hour. The TCD determined the amount of hydrogen consumed in the tail gas stream. The TPR peaks show the reducible catalyst species. To study the basic property of the catalyst, CO_2-TPD analysis was carried out using the same instrument as the TPR studies. The calcined catalyst was first treated for 50 min at 250 °C with He flow. The CO_2 sorption process was then started up again by letting CO_2 flow at 10 mL/min for 30 min at 75 °C. CO_2 was removed from the sorbent bed by passing He gas through it at a rate of 20 mL/min, while gradually raising the temperature from 40 °C to 950 °C at a rate of 10 °C/min. During the ramping sequence, the temperature was kept at °C for 20 min. The acidity of the catalyst was determined using TPD-NH_3. The catalyst was preheated at 250 °C for 20 min under He flow. The temperature was then reduced to 170 °C, and the flow was changed from He to NH_3 for 30 min. Then, the flow was changed back to He for 20 min. After the NH_3 dosage was completed, the temperature was subsequently ramped up to 950 °C under He flow at 10 °C/min.

3.3. Catalyst Performance Evaluation

The catalytic activity evaluation was carried out in a tubular, stainless steel fixed-bed reactor (Effi Microactivity reactor, PID Eng & Tech, Norcross, GA, USA). Prior to the reaction, 0.2 g of calcined catalyst was activated in H_2 flow of 20 mL/min at 250 °C and 400 °C. The reaction was then carried out at 22.5 bar, 250 °C, and CO_2:H_2 (1:3), with a total flow rate of 36 mL/min for 5 h. The reactor effluents were analyzed using a gas chromatograph, equipped with a TCD detector for H_2 and CO_2 analysis and an FID detector for alcohols and other hydrocarbons. CO_2 conversion and methanol selectivity were calculated using Equations (2) and (3), respectively.

$$\text{CO}_2 \text{ Conversion } (\%) = \frac{\text{Moles of CO}_{2\text{ in}} - \text{Moles of CO}_{2\text{ out}}}{\text{Moles of CO}_{2\text{ in}}} \times 100 \quad (2)$$

$$\text{MeOH Selectivity } (\%) = \frac{\text{Moles of MeOH produced}}{\text{Total moles of products}} \times 100 \quad (3)$$

4. Conclusions

A Tri-promoted Cu/ZnO catalyst, supported on Al_2O_3 and SBA-15, favored the formation of methyl formate from the CO_2 hydrogenation reaction conducted at 22.5 bar, 250 °C, and CO_2:H_2 (1:3). The selectivity of methyl formate was 93.52% and 77.94%, respectively, over the Cu/ZnO/SBA-15 and Cu/ZnO/Al_2O_3 catalysts when the catalysts were reduced at 250 °C. However, the selectivity of methyl formate decreased to 64.47% (CZMNZA) and 91.65% (CZMNZS) with 400 °C reduction temperature. The catalytic activity and methanol selectivity were approximately higher by a factor of five and twelve, respectively, on the Al_2O_3-supported catalyst compared to the values obtained using the SBA-15-supported catalyst.

Author Contributions: Conceptualization, N.A.M.Z.; methodology, N.H.B. and N.A.S.; formal analysis, N.H.B. and N.A.S.; writing—original draft preparation, N.H.B.; writing—review and editing, N.H.B. and N.A.M.Z.; visualization, N.H.B.; supervision, N.A.M.Z.; funding acquisition, N.A.M.Z. All authors have read and agreed to the published version of the manuscript.

Funding: This research was funded by the MRA Research Grant (cost center: 015MDO-031).

Data Availability Statement: No additional data provided.

Acknowledgments: The authors acknowledge the support provided by Universiti Teknologi PETRONAS and PETRONAS Research Sdn. Bhd.

Conflicts of Interest: The authors declare no conflict of interest.

References

1. Wang, W.; Wang, S.; Ma, X.; Gong, J. Recent advances in catalytic hydrogenation of carbon dioxide. *Chem. Soc. Rev.* **2011**, *40*, 3703–3727. [CrossRef]
2. Olah, G.A. Beyond oil and gas: The methanol economy. *Angew. Chem. Int. Ed. Engl.* **2005**, *44*, 2636–2639. [CrossRef]
3. Graciani, J.; Mudiyanselage, K.; Xu, F.; Baber, A.E.; Evans, J.; Senanayake, S.D.; Stacchiola, D.J.; Liu, P.; Hrbek, J.; Fernández Sanz, J.; et al. Highly active copper-ceria and copper-ceria-titania catalysts for methanol synthesis from CO_2. *Science* **2014**, *345*, 546–550. [CrossRef]
4. Ortelli, E.E.; Wambach, J.; Wokaun, A. Methanol synthesis reactions over a CuZr based catalyst investigated using periodic variations of reactant concentrations. *Appl. Catal. A Gen.* **2001**, *216*, 227–241. [CrossRef]
5. Chinchen, G.C.; Denny, P.J.; Jennings, J.R.; Spencer, M.S.; Waugh, K.C. Synthesis of methanol: Part 1. Catalysts and kinetics. *Appl. Catal.* **1988**, *36*, 1–65. [CrossRef]
6. Fujita, S.I.; Usui, M.; Ito, H.; Takezawa, N. Mechanisms of methanol synthesis from carbon dioxide and from carbon monoxide at atmospheric pressure over Cu/ZnO. *J. Catal.* **1995**, *157*, 403–413. [CrossRef]
7. Spencer, M.S. The role of zinc oxide in Cu/ZnO catalysts for methanol synthesis and the water-gas shift reaction. *Top. Catal.* **1999**, *8*, 259–266. [CrossRef]
8. Behrens, M.; Studt, F.; Kasatkin, I.; Kühl, S.; Hävecker, M.; Abild-Pederson, F.; Zander, S.; Girgsdies, S.; Kurr, P.; Kniep, B.L.; et al. The active site of methanol synthesis over Cu/ZnO/Al_2O_3 industrial catalysts. *Science* **2012**, *336*, 893–897. [CrossRef]
9. Ali, K.A.; Abdullah, A.Z.; Mohamed, A.R. Recent development in catalytic technologies for methanol synthesis from renewable sources: A critical review. *Renew. Sustain. Energy Rev.* **2015**, *44*, 508–518. [CrossRef]
10. Fujitani, T.; Nakamura, J. The chemical modification seen in the Cu/ZnO methanol synthesis catalysts. *Appl. Catal. A Gen.* **2000**, *191*, 111–129. [CrossRef]
11. Liu, X.M.; Lu, G.Q.; Yan, Z.F.; Beltramini, J. Recent advances in catalysts for methanol synthesis via hydrogenation of CO and CO_2. *Ind. Eng. Chem. Res.* **2003**, *42*, 6518–6530. [CrossRef]
12. Dong, X.; Zhang, H.B.; Lin, G.D.; Yuan, Y.Z.; Tsai, K.R. Highly active CNT-Promoted Cu-ZnO-Al_2O_3 catalyst for methanol synthesis from $H_2/CO/CO_2$. *Catal. Lett.* **2003**, *85*, 237–246. [CrossRef]
13. Ayodele, O.B.; Tasfy, S.F.H.; Zabidi, N.A.M.; Uemura, Y. Co-synthesis of methanol and methyl formate from CO_2 hydrogenation over oxalate ligand functionalized ZSM-5 supported Cu/ZnO catalyst. *J. CO_2 Util.* **2017**, *17*, 273–283. [CrossRef]
14. Tasfy, S.F.H.; Zabidi, N.A.M.; Shaharun, M.S.; Subbarao, D. The role of support morphology on the performance of Cu/ZnO-catalyst for hydrogenation of CO_2 to methanol. In *AIP Conference Proceedings, Proceedings of the 23rd Scientific Conference of Microscopy Society Malaysia, Tronoh, Malaysia, 10–12 December 2014*; Hussain, P., Bhat, A.H., Chowdury, S., Mohamed, N.M., Othman, F., Mamat, O., Eds.; AIP Publishing: Woodbury, NY, USA, 2015. [CrossRef]
15. Zabidi, N.A.M.; Tasfy, S.F.H.; Shaharun, M.S. Effects of Nb promoter on the properties of Cu/ZnO/SBA-15 catalyst and performance in methanol production. *Key Eng. Mater.* **2016**, *708*, 94–97. [CrossRef]
16. Tasfy, S.F.H.; Zabidi, N.A.M.; Shaharun, M.S.; Subbarao, D. Effect of Mn and Pb promoters on the performance of Cu/ZnO-Catalyst in CO_2 hydrogenation to methanol. *Appl. Mech. Mater.* **2014**, *625*, 289–292. [CrossRef]

17. Zhan, H.; Li, F.; Gao, P.; Zhao, N.; Xiao, F.; Wei, W.; Zhong, L.; Sun, Y. Methanol synthesis from CO_2 hydrogenation over La–M–Cu–Zn–O (M = Y, Ce, Mg, Zr) catalysts derived from perovskite-type precursors. *J. Power Source.* **2014**, *251*, 113–121. [CrossRef]
18. Tada, S.; Watanabe, F.; Kiyota, K.; Shimoda, N.; Hayashi, R.; Takahashi, M.; Nariyuki, A.; Igarashi, A.; Satokawa, S. Ag addition to CuO-ZrO_2 catalysts promotes methanol synthesis via CO_2 hydrogenation. *J. Catal.* **2017**, *351*, 107–118. [CrossRef]
19. Słoczyński, J.; Grabowski, R.; Olszewski, P.; Lachowska, M.; Skrzypek, J.; Stoch, J. Effect of Mg and Mn oxide additions on structural and adsorptive properties of Cu/ZnO/ZrO_2 catalysts for the methanol synthesis from CO_2. *Appl. Catal. A Gen.* **2003**, *249*, 129–138. [CrossRef]
20. Li, S.; Guo, L.; Ishihara, T. Hydrogenation of CO_2 to methanol over Cu/AlCeO catalyst. *Catal. Today* **2019**, *339*, 352–361. [CrossRef]
21. Huang, C.; Wen, J.; Sun, Y.; Zhang, M.; Bao, Y.; Zhang, Y.; Liang, L.; Fu, M.; Wu, J.; Ye, D.; et al. CO_2 hydrogenation to methanol over Cu/ZnO plate model catalyst: Effects of reducing gas induced Cu nanoparticle morphology. *Chem. Eng. J.* **2019**, *374*, 221–230. [CrossRef]
22. Fujitani, T. Enhancement of the catalytic performance and active site clarification of Cu/ZnO based catalysts for methanol synthesis by CO_2 hydrogenation. *J. Jpn. Pet. Inst.* **2020**, *63*, 43–51. [CrossRef]
23. Din, I.U.; Shaharun, M.S.; Naeem, A.; Tasleem, S.; Johan, M.R. Carbon nanofiber-based copper/zirconia catalyst for hydrogenation of CO_2 to methanol. *J. CO_2. Util.* **2017**, *21*, 145–155. [CrossRef]
24. Chen, C.S.; Cheng, W.H.; Lin, S.S. Study of reverse water gas shift reaction by TPD, TPR and CO_2 hydrogenation over potassium-promoted Cu/SiO_2 catalyst. *Appl. Catal. A Gen.* **2003**, *238*, 55–67. [CrossRef]
25. Kaiser, D.; Beckmann, L.; Walter, J.; Bertau, M. Conversion of green methanol to methyl formate. *Catalysts* **2021**, *11*, 869. [CrossRef]
26. Barrett, E.P.; Joyner, L.G.; Halenda, P.P. The determination of pore volume and area distributions in porous substances. I. Computations from nitrogen isotherms. *J. Am. Chem. Soc.* **1951**, *73*, 373–380. [CrossRef]
27. Tasfy, S.F.H.; Zabidi, N.A.M.; Shaharun, M.S. Methanol production via CO_2 hydrogenation reaction: Effect of catalyst support. *Int. J. Nanotechnol.* **2017**, *14*, 410–421. [CrossRef]
28. Tasfy, S.F.H. Development and Performance Analysis of Cu-ZnO/SBA-15 Catalysts for Hydrogenation of Carbon Dioxide to Methanol. Ph.D. Thesis, Universiti Teknologi Petronas, Seri Iskandar, Malaysia, 2016.
29. Halim, N.S.A. Synthesis, Characterization and Performance of Copper-Zinc Oxide with Mixed Promoter Catalyst for CO_2 Hydrogenation to Methanol. Master's Thesis, Universiti Teknologi Petronas, Seri Iskandar, Malaysia, 2019.
30. Huang, C.; Chen, S.; Fei, X.; Liu, D.; Zhang, Y. Catalytic hydrogenation of CO_2 to methanol: Study of synergistic effect on adsorption properties of CO_2 and H_2 in CuO/ZnO/ZrO_2 system. *Catalysts* **2015**, *5*, 1846–1861. [CrossRef]
31. Li, Z.; Yan, S.; Fan, H. Enhancement of stability and activity of Cu/ZnO/Al_2O_3 catalysts by microwave irradiation for liquid phase methanol synthesis. *Fuel* **2013**, *106*, 178–186. [CrossRef]
32. Lu, Q.; Wang, Z.; Li, J.; Wang, P.; Ye, X. Structure and photoluminescent properties of ZnO encapsulated in mesoporous silica SBA-15 fabricated by two-solvent strategy. *Nanoscale Res. Lett.* **2009**, *4*, 646–654. [CrossRef] [PubMed]
33. Wang, Z.; Chen, B.; Quan, G.; Li, F.; Wu, Q.; Dian, L.; Dong, Y.; Li, G.; Wu, C. Increasing the oral bioavailability of poorly water-soluble carbamazepine using immediate-release pellets supported on SBA-15 mesoporous silica. *Int. J. Nanomed.* **2012**, *7*, 5807–5818. [CrossRef]
34. Zhao, D.; Feng, J.; Melosh, N.; Fredrickson, G.H.; Chmelka, B.F.; Stucky, G.D. Triblock copolymer syntheses of mesoporous silica with periodic 50 to 300 angstrom pores. *Science* **1998**, *279*, 548–552. [CrossRef] [PubMed]
35. Nguyen, Q.N.K.; Yen, N.T.; Hau, N.D.; Tran, H.L. Synthesis and characterization of mesoporous silica SBA-15 and ZnO/SBA-15 photocatalytic materials from the ash of brickyards. *J. Chem.* **2020**, *2020*, 8456194. [CrossRef]
36. Le, H.V.; Parishan, S.; Sagaltchik, A.; Ahi, H.; Trunschke, A.; Schomäcker, R.; Thomas, A. Stepwise methane-to-methanol conversion on CuO/SBA-15. *Chem.—A Eur. J.* **2018**, *24*, 12592–12599. [CrossRef]
37. Mao, D.; Zhang, J.; Zhang, H.; Wu, D. A highly efficient Cu-ZnO/SBA-15 catalyst for CO_2 hydrogenation to CO under atmospheric pressure. *Catal. Today* **2022**, *402*, 60–66. [CrossRef]
38. Liu, W.; Sarofim, A.; Flytzani-Stephanopoulos, M. Complete oxidation of carbon monoxide and methane over metal-promoted fluorite oxide catalysts. *Chem. Eng. Sci.* **1994**, *49*, 4871–4888. [CrossRef]
39. Din, I.; Shaharun, M.S.; Subbaro, D.; Naeem, A.; Hussain, F. Influence of niobium on carbon nanofibres based Cu/ZrO_2 catalysts for liquid phase hydrogenation of CO_2 to methanol. *Catal. Today* **2016**, *259*, 303–311. [CrossRef]
40. Jones, J.R.; Sharratt, A.P.; Jackson, S.D.; Griffiths, R.W.; Gladden, L.F.; Robertson, F.J.; Webb, G. Temperature-programmed reduction of nickel/silica catalysts using [^{3}H]-hydrogen. *J. Radioanal. Nucl. Chem.* **1992**, *166*, 69–74. [CrossRef]
41. Tkachenko, O.P.; Klementiev, K.V.; van den Berg, M.W.E.; Koc, N.; Bandyopadhyay, M.; Birkner, A.; Wöll, C.; Gies, H.; Grünert, W. Reduction of copper in porous matrixes. Stepwise and autocatalytic reduction routes. *J. Phys. Chem. B* **2005**, *109*, 20979. [CrossRef]
42. Suprun, W.; Lutecki, M.; Haber, T.; Papp, H. Acidic catalysts for the dehydration of glycerol: Activity and deactivation. *J. Mol. Catal. A Chem.* **2009**, *309*, 71–78. [CrossRef]
43. Tursunov, O.; Kustov, L.; Tilyabaev, Z. Methanol synthesis from the catalytic hydrogenation of CO_2 over CuO–ZnO supported on aluminum and silicon oxides. *J. Taiwan Inst. Chem. Eng.* **2017**, *78*, 416–422. [CrossRef]
44. Venkata, D.B.C.; Likozar, B. The role of copper oxidation state in Cu/ZnO/Al_2O_3 catalysts in CO_2 hydrogenation and methanol productivity. *Renew. Energy* **2019**, *140*, 452–460. [CrossRef]

45. Koh, M.K.; Wong, Y.J.; Chai, S.P.; Mohamed, A.R. Carbon dioxide hydrogenation to methanol over multi-functional catalyst: Effects of reactants adsorption and metal-oxide(s) interfacial area. *J. Ind. Eng. Chem.* **2018**, *62*, 156–165. [CrossRef]
46. Gao, P.; Li, F.; Zhao, N.; Xiao, F.; Wei, W.; Zhong, L. Influence of modifier (Mn, La, Ce, Zr and Y) on the performance of Cu/Zn/Al catalysts via hydrotalcite-like precursors for CO_2 hydrogenation to methanol. *Appl. Catal. A Gen.* **2013**, *468*, 442–452. [CrossRef]
47. Liu, Y.; Sun, K.; Ma, H.; Xu, X.; Wang, X. Cr, Zr-incorporated hydrotalcites and their application in the synthesis of isophorone. *Catal. Commun.* **2010**, *11*, 880–883. [CrossRef]
48. Cannilla, C.; Bonura, G.; Rombi, E.; Arena, F.; Frusteri, F. Highly effective MnCeOx catalysts for biodiesel production by transesterification of vegetable oils with methanol. *Appl. Catal. A Gen.* **2010**, *382*, 158–166. [CrossRef]
49. van den Berg, M.W.E.; Polarz, S.; Tkachenko, O.P.; Klementiev, K.V.; Bandyopadhyay, M.; Khodeir, L.; Gies, H.; Muhler, M.; Grünert, W. Cu/ZnO aggregates in siliceous mesoporous matrices: Development of a new model methanol synthesis catalyst. *J. Catal.* **2006**, *241*, 446–455. [CrossRef]
50. Kattel, S.; Ramírez, P.J.; Chen, J.G.; Rodriguez, J.A.; Liu, P. Response to comment on active sites for CO_2 hydrogenation to methanol on Cu/ZnO catalysts. *Science* **2017**, *357*, 8210. [CrossRef]
51. Witoon, T.; Chalorngtham, J.; Dumrongbunditkul, P.; Chareonpanich, M.; Limtrakul, J. CO_2 hydrogenation to methanol over Cu/ZrO_2 catalysts: Effects of zirconia phases. *Chem. Eng. J.* **2016**, *293*, 327–336. [CrossRef]
52. Fujita, S.-I.; Moribe, S.; Kanamori, Y.; Kakudate, M.; Takezawa, N. Preparation of a coprecipitated Cu/ZnO catalyst for the methanol synthesis from CO_2—effects of the calcination and reduction conditions on the catalytic performance. *Appl. Catal. A Gen.* **2001**, *207*, 121–128. [CrossRef]
53. Kobl, K.; Angelo, L.; Zimmermann, Y.; Sall, S.; Parkhomenko, K.; Roger, A.C. In situ infrared study of formate reactivity on water-gas shift and methanol synthesis catalysts. *Comptes Rendus Chim.* **2015**, *18*, 302–314. [CrossRef]
54. Chen, Y.; Choi, S.; Thompson, L.T. Ethyl formate hydrogenolysis over Mo_2C-based catalysts: Towards low temperature CO and CO_2 hydrogenation to methanol. *Catal. Today* **2016**, *259*, 285–291. [CrossRef]
55. Indu, B.; Ernst, W.R.; Gelbaum, L.T. Methanol-formic acid esterification equilibrium in sulfuric acid solutions: Influence of sodium salts. *Ind. Eng. Chem. Res.* **1993**, *32*, 981–985. [CrossRef]